RSC Advances

ROYAL SOCIETY OF CHEMISTRY

www.rsc.org/advances

RSCAdvances

Dynamic Article Links ▶

PAPER

Structural, transport, magnetic and magnetoelectric properties of CaMn$_{1-x}$Fe$_x$O$_{3-\delta}$ (0.0 ≤ x ≤ 0.4)

Brajendra Singh*

We have investigated the structural, magnetic, transport and magnetoelectric properties of parent and Fe doped CaMn$_{1-x}$Fe$_x$O$_{3-\delta}$ (0.0 ≤ x ≤ 0.4) manganites using synchrotron X-ray, Raman, squid and nova control impedance analyzer. Fe doped composition x=0.3 show strong Maxwell-Wagner effect and quite high positive magnetocapacitance (MC) ~ 8.45% at room temperature at low magnetic field 7.8kG has 10 been observed. Rietveld refinement of synchrotron X-ray diffraction patterns suggests (i) the structural transformation from orthorhombic to cubic crystal system and (ii) increase in lattice parameters with the substitution of Fe at Mn site. Sintering at 1300°C stabilizes doping of higher ionic radii Fe^{+3} (0.645Å)/ Fe^{+4} (0.585Å) atoms at Mn^{+4} (0.53Å) site in CaMn$_{1-x}$Fe$_x$O$_{3-\delta}$. The Magnetization data shows the transformation of G type of antiferromagnetic arrangement of Mn^{+4} electrons spins in CaMnO$_3$ into 15 paramagnetic spin type arrangement with the Fe substitution. AC conductivity of Fe doped compositions decreases more than two orders of magnitude in comparison to CaMnO$_{3-\delta}$.

Introduction

A strong coupling between magnetic and electronic degree of freedoms makes mixed valence (Mn^{+4}/Mn^{+3}) containing 20 perovskite manganites to show various important properties like colossal magneto resistance, metal to insulator transition, ferromagnetic to paramagnetic transition, charge ordering phenomenon.[1-2] Magnetic exchange interactions can be controlled by the ratio of Mn^{+4}(0.53Å)/Mn^{+3}(0.645Å) mixed 25 valence states, involves the e$_g$ hopping of electrons, explained using double exchange (DE) mechanism in perovskite manganites.[3] It has been found that operative DE mechanism due to the redox interactions of Mn^{+3}/Mn^{+4} facilitated by the redox pair Ru^{+4}/Ru^{+5} in perovskite manganites.[4] When lower size atom 30 Ca^{+2}(1.34Å) doped at Sr^{+2} (1.44Å) site in Sr$_{1-x}$Ca$_x$MnO$_3$, crystal structure changes form orthorhombic to tetragonal to cubic.[5] Recently, a large magnetodielectric response around the magnetic phase transition has been reported in perovskite containing Mn and Ni or Fe ions, GdMnO$_3$, TbMnO$_3$ and DyMnO$_3$.[6-9] A large 35 increase in the dielectric constant was also reported in the phase separated Pr$_{0.67}$Ca$_{0.33}$MnO$_3$ at low temperatures.[10] A dielectric resonance has been observed in perovskite manganite La$_{2/3}$Ca$_{1/3}$MnO$_3$ at 0.5T magnetic field in the paramagnetic regime just above the ferromagnetic temperature at 270K.[11] 40 Moreover, Rairigh et al. observed a colossal magnetocapacitance coinciding with a regime of phase separation between magnetic metal and charge ordered insulating phase at low temperatures.[12] Several systems show magnetocapacitance (MC) effect without the presence of spontaneous electric polarization and 45 magnetization.[13-14] However, these MC effects are below 1%

under a strong magnetic field of several tesla. The origin of such effects understood through the Maxwell-Wagner relaxation model developed for inhomogeneous semiconductors.[15] According to Maxwell-Wagner effects, presence of 50 inhomogeniety or contact effects in materials can enhance the dielectric constant and yield dielectric relaxation in the absence of intrinsic dipolar relaxation.[16-17] It has been also found that the Maxwell- Wagner effect can also yield a magnetocapacitance without multiferroicity and saturated magnetization, provided the 55 material exhibits an intrinsic magnetoresistance.[15] A recent theoretical prediction suggests the possible occurrence of the magnetocapacitance effect even in the non magnetic composite media.[18] Materials with magnetocapacitance property, can have various potential applications.[19] However, the challenge is to 60 search a material which show magnetocapacitance within the ideal frequency range ω < 1MHz at room temperature for magnetic field (H) < 1Tesla. Perovskite manganite materials may play a major role and might be the potential candidate for the applications in magnetic sensors, miniaturization of antenna, spin 65 charge transducers and microwave tunable filters.[1-2] In this manuscript, we show the doping of Fe at Mn site in CaMnO$_{3-\delta}$ upto 40%. Further, Fe doping induced structural transformation, magnetic and ac transport studies of parent and Fe doped manganites CaMn$_{1-x}$Fe$_x$O$_{3-\delta}$ (0.0 ≤ x ≤ 0.4), and quit high 70 magnetocapacitance (MC) value at low magnetic field at low frequency and at room temperature has been reported.

Experimental Section

Polycrystalline samples CaMn$_{1-x}$Fe$_x$O$_{3-\delta}$ (0.0 ≤ x ≤ 0.4) were prepared using high temperature solid state reaction route. The

stoichiometric amount of $CaCO_3$, MnO_2 and Fe_2O_3 were thoroughly mixed in an agate mortar and calcined at 950°C for 48 hours by keeping heating rate 10°C/min and cooling rate 5°C/min. After calcinations, powders were pelletized into 10 mm diameter

5 and sintered in ambient atmosphere at 1300°C for 24 hours by keeping heating rate 10°C/min and cooling rate 5°C/min. We have noticed the colour of $CaMnO_3$ pellet is gray while Fe doped compositions pellet are in black colour. The Synchrotron X-ray powder diffraction patterns were recorded at room temperature

10 using Synchrotron radiation at Indian beamline, Photon Factory (PF), KEK, Japan. Synchrotron x-ray beam (wavelength - 1.09Å) from the bending magnet of the PF storage ring was first focused horizontally with a focusing mirror and then monochromatized using a double-crystal monochromator. The beam was then

15 further collimated with a set of beam-defining slits having horizontal openings of 2 mm and 0.2 mm in the vertical direction. The sample was mounted onto an 8-circle goniometer (Huber, Germany) at the focal point of the focusing mirror of the beamline. The sample was mounted horizontally and the scattered

20 beam was collected by a single-channel scintillation detector mounted at a distance of 380 cm onto the 2h arm of the goniometer. A slit of 1.5mm (horizontal) by 0.25mm (vertical) was mounted just before the detector to increase the signal-to-background ratio. Rietveld refinements were done using Fullprof

25 software. Raman measurements on the pelletized samples were performed using a Raman microprobe instrument consisting of a Jobin-Yvon T64000 spectrometer equipped with a microscope which allows a spatial resolution on the sample of about 1 μm. Raman signal was detected by a multichannel CCD detector.

30 Excitation wavelength of 514.5 nm was used with 3.0 mW power to carry out the experiments. We have recorded each sample data for 5 minutes in the range of 90 – 900 cm^{-1} at room temperature. To improve the resolution of closely spaced peaks, high-resolution scans were recorded using the triple additive

35 configuration, with a spectral resolution better than 1 cm^{-1}. Iodometric titration was performed on 10-30 mg of samples to determine the mean valency of Mn and Fe. The sample was weighed in round neck vessel. An excess of potassium iodide with distil water added. Solution was flushed with Ar to avoid air

40 oxidation of excess iodide. After adding HCl, sealed vessel heated to dissolve the sample. The sample was cooled and titrated with standardized sodium thiosulphate. Freshly prepared Starch solution was used as an indicator. This gave mean valency of Mn and Fe and the amount of oxygen was then calculated.

45 Magnetization of the samples was recorded using SQUID in the temperature range 10K – 300K at 1Tesla applied magnetic field. Magnetocapacitance (MC) measurements were recorded using nova control-Impedance analyzer in the frequency range from 1Hz to 40 MHz and using DC electromagnet.

50 Magnetocapacitance (MC%) and magnetoloss (ML%) calculated by the respective formula $(C(H) – C(0))$ x $100/C(0)$, $(D(H) – D(0))$ x $100/D(0)$ where $C(H)/D(H)$ is the capacitance/dielectric loss in presence of DC magnetic field in kilo Gauss and $C(0)/D(0)$ is the capacitance/dielectric loss in absence of

55 magnetic field.

Results and Discussion

Synchrotron X-ray diffraction (XRD) patterns are shown in
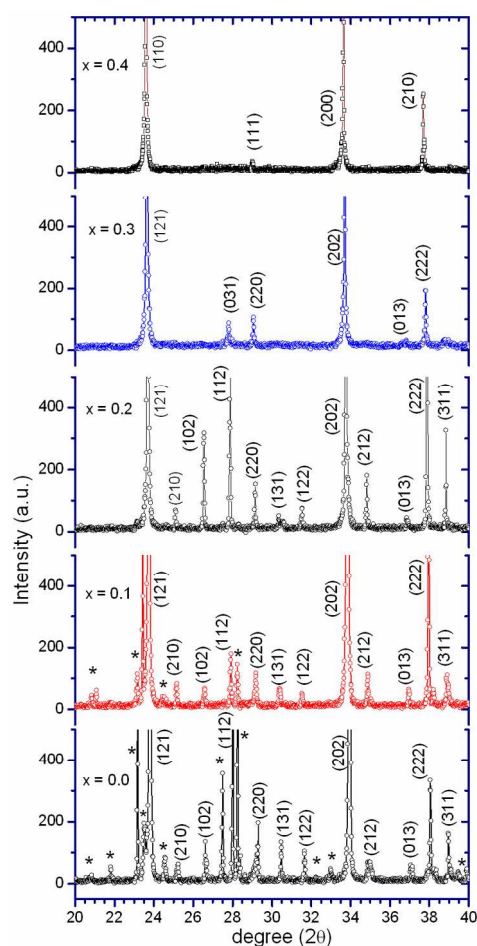
Figure 1. Synchrotron x-ray diffraction patterns for $CaMn_{1-x}Fe_xO_{3-\delta}$ ($0.0 \leq x \leq 0.4$). * shows the extra peaks originated by oxygen nonstoichiometry.
60 Note the absence of extra peaks for x=0.2, 0.3 and 0.4 compositions.

Figure 1 for $CaMn_{1-x}Fe_xO_{3-\delta}$ ($0.0 \leq x \leq 0.4$). Parent composition x=0.0 shows some extra peaks indicated by *, originated due to the oxygen nonstoichiometry in the lattice. We have also found grey colour of our Parent $CaMnO_{3-\delta}$ sample, which is the

65 signature of the oxygen nonstoichiometry in $CaMnO_3$ lattice.[20-23] Reller et al.[20] has shown that in the ideal structure of perovskite, the creation of one anion vacancy (removal of one oxygen) causes the reduction of two Mn^{+4} cations to two Mn^{+3} cations and simultaneously two MnO_6 octahedra are transformed into two

70 MnO_5 square-pyramids. The number of oxygen vacancies i.e. the value of δ in the stoichiometric formula $CaMnO_{3-\delta}$ represents therefore a direct measure for the ratios Mn^{+4}/Mn^{+3} and MnO_6 octahedra/MnO_5 square-pyramids respectively. We have found the oxygen content was greater than 2.5 in x=0.0 composition

75 after comparing with the XRD pattern of $CaMnO_{2.5}$.[20-23] Manganites are known to have mixed valences of Mn and in presence of oxygen deficiency, the Mn^{+4} valence state reduces into Mn^{+3} for charge valence in lattice.[24] In presence of Jahn teller (JT) ion Mn^{+3}, lattice distortion is expected in $CaMnO_{3-\delta}$. In

80 fact, the new peaks shown in X-ray diffraction pattern by *, clearly indicate the distortion of lattice due to the Jahn teller ion Mn^{+3} and the presence of MnO_6 octahedra along with the MnO_5 square-pyramids .[20-21] We have compared XRD patterns with the all possible phases (CaO, MnO_2,Mn_2O_3, Mn_3O_4-JCPDS XRD

patterns given in supplementary information) which might originated as impurity phase but we have not found any similarity of them. So, conclusively new peaks in x=0.0 composition are generated due to the presence of Jahn teller ion Mn^{+3} and MnO_5
5 square-pyramids. Similarly, Fe doped composition x=0.1 also show the presence of extra peaks in diffraction patterns.[25] With Fe doping, these extra peaks are reduced in x=0.1, which shows the less distortion in lattice and it might be due to the presence of non JT Fe^{+3} $(t_{2g}^3 e_g^2)$ valence state in lattice. Further, We have
10 observed the shift in the peaks towards lower theta value with the increase in Fe content, which shows the increase in the lattice constants with the increase in Fe content. Increased lattice constant for x=0.1 in comparison to x=0.0 composition and equal ionic radii of Mn^{+3} (0.645Å) and Fe^{+3} (0.645Å) suggest that
15 oxygen content in both the compositions is > 2.9. We have found the systematic changes in the diffraction patterns with the increase in Fe doping, which infers the change in structure. The compositions (x = 0.0, 0.1 and 0.2) show a number of super lattice reflections (R,M.X), which are the characteristic peaks for
20 the orthorhombic crystal structure. Peaks (210), (102) and (112) are similar with the X, M and R point distortions found in Mn and Zr based perovskite materials.[22, 26,27] The super lattice reflections R, M and X in $CaMn_{1-x}Fe_xO_3$ (x = 0.0, 0.1 and 0.2) originate due to the rotation of MnO_6 octahedra in the orthorhombic perovskite
25 manganites. Reflections due to the out of phase or (-) rotations of MnO_6 octahedra are called R-point distortions and in-phase or (+) rotations of octahedral are termed as M-point reflections. X-point distortions occur when R-point and M-point distortions operate in concert. These super lattice reflections are similar to Glazer tilt
30 system $(a^+b^-b^-)$, which corresponds to the orthorhombic crystal system. On increasing the Fe substitution at Mn site, the M-point reflections are no longer observed in $CaMn_{0.7}Fe_{0.3}O_3$. The XRD patterns of these x = 0.2 composition resembles the XRD patterns of manganites compounds having Pnma space group.[28] The XRD
35 pattern of composition x=0.2 shows no extra peaks in diffraction peaks which shows there is no oxygen deficiency in lattice. While for x = 0.3 composition, we have neither observed (R, M, X) super lattice reflections nor extra peaks. XRD patterns resemble the diffraction patterns of Imma space group containing
40 manganite compounds. The XRD peaks of the composition x = 0.4 are regularly spaced without the extra peaks, which shows the higher symmetry of the crystal system. Absence of extra reflections in x=0.2, 0.3 and 0.4 show that there is no oxygen non stoichiometry and only Mn^{+4}/Fe^{+4} valence states present in lattice.
45 We have done reitveld analysis of these compositions and found that x=0.2 composition crystallize in Pnma, x=0.3 in Imma and x=0.4 in cubic space group Pm-3m (Figure 2 and Table 1). It is reported in literature that if tolerance factor value [t = $(r_A + r_O)/\sqrt{2}(r_B + r_O)$] is close to 1 then perovskite structure is found
50 to be cubic. If t is ≤ 0.95 then it is found to be Orthorhombic. In this case, the tolerance factor is found to be 1 for x=0.4 composition only if Fe is present in lattice as Fe^{+4}. Fe^{+4} has ionic radii 0.585Å and Fe^{+3} has ionic radii 0.645Å . So if Fe^{+3} will be present in lattice than tolerance factor value does not support the
55 cubic crystal structure for x=0.4 composition. The results of Synchrotron XRD patterns show the change in crystal system on increasing the Fe content at Mn site in $CaMn_{1-x}Fe_xO_3$. These observations are similar with the phase transitions in
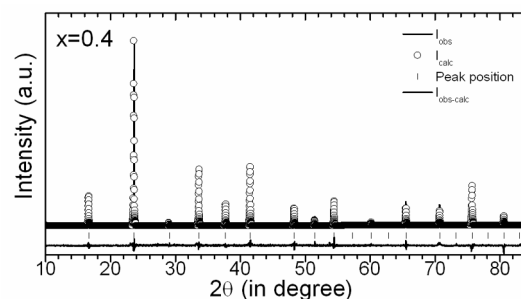
60

Figure 2. Rietveld refinement results of synchrotron x-ray diffraction pattern for $CaMn_{0.6}Fe_{0.4}O_3$. The experimental data points are shown as circles, and the calculated fit and difference curve are shown as solid lines. Tick marks indicate the calculated reflection positions. Bragg R
65 factor and R_F is found 6.1 and 10.5 respectively.

Table 1: Lattice parameters as determined by rietveld refinement of synchrotron x-ray diffraction patterns

$CaMn_{1-x}Fe_xO_{3-\delta}$	x=0.2	x=0.3	x=0.4
Space Group	Pnma	Imma	Pm-3m
a (Å)	5.30149(9)	5.3146(2)	3.7683(9)
b (Å)	7.49622(11)	7.5178(3)	3.7683(9)
c(Å)	5.2956(2)	5.2959(2)	3.7683(9)

75 $Sr_{1-x}Ca_xMnO_3$ perovskites,[5,29] where lower atomic size Ca atom doped at bigger atomic size Sr site. Our reported results are different from reported results in literature by Liu et al. where they had reported Pnma orthorhombic crystal structure up to x=0.35 doping of Fe.[30] The difference in the structural properties
80 is found due to different (i) precursors used (ii) synthesizing method and (iii) sequence of sintering temperature. Crystal structure of perovskites is very sensitive to the sintering temperatures. The calcination and sintering temperature, quenching, heating and cooling rate, sintering time, sintering in
85 oxidation/reduction/ambient atmosphere, these are some of the factors by which the structure, oxygen stoichiometry, crystal structure and physical properties of perovskite can be controlled. To prepare bilayer manganites $(La,Sr/Ca)_3Mn_2O_7$, which are a stack resembling spin valve devices due to the Mn-O-Mn
90 network separated by insulating $(La,Sr/Ca)_2O_2$ spacer layer along with the c-axis, precursors has to be sintered >1400°C.[31] If it will be sintered lower than this temperature than layered manganite does not form. Briatico et al. have purposefully prepared the oxygen deficient $CaMnO_{3-\delta}$ (0 ≤ δ ≤ 0.34) to explore the electrical
95 resistivity in oxygen deficient compounds. [32] In our case, we have sintered at high temperature (1300°C) to stabilize the rare valence state phase in Fe doped $CaMnO_{3-\delta}$ compositions.

Raman spectroscopy has been efficiently applied for monitoring the structural changes and Jahn-Teller disorder in manganites at
100 microscopic levels. In mixed-valence manganites, Jahn-Teller distortion is found due to the presence of one e_g electron of Mn^{+3} and oxygen sub lattice is remains highly distorted. Due to these effects, when its Raman spectra is compared to undistorted structure's spectra then such effects arise (i) broadening of some
105 or all first-order Raman lines (ii) activation in the Raman spectrum of otherwise forbidden phonon modes, and (iii) the appearance of additional broad Raman bands.[33-35] According to
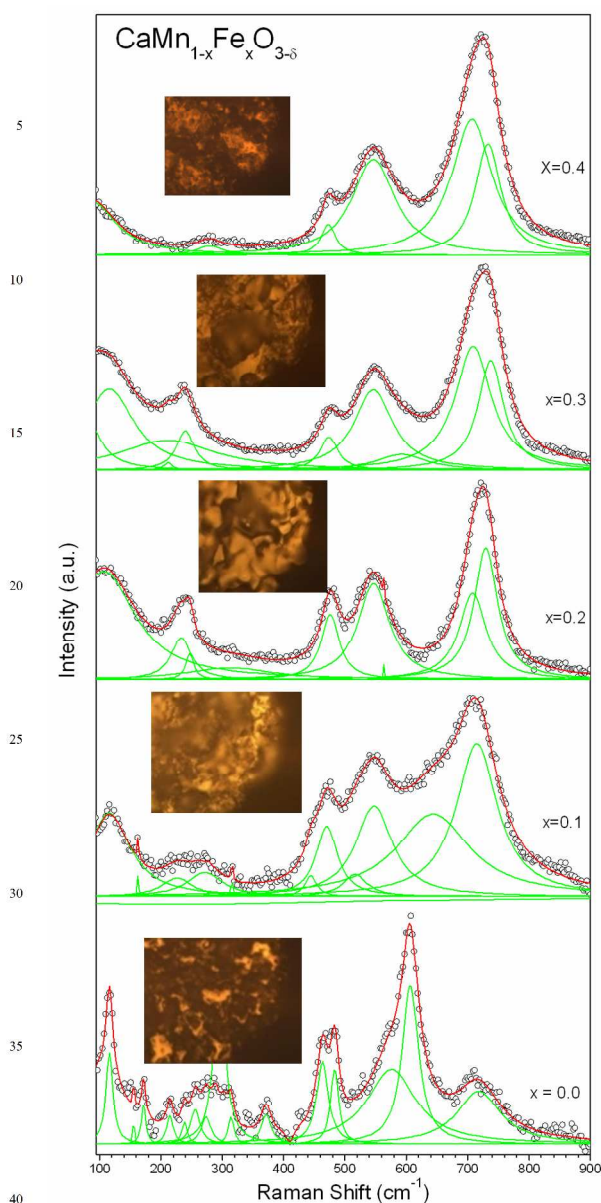
Figure 3. Raman spectroscopy measurements for $CaMn_{1-x}Fe_xO_{3-\delta}$ ($0.0 \leq x \leq 0.4$). Circles show the recorded data while red line shows the whole fitting, green lines shows the position of individual peaks. Images recorded by microscope to show the samples surface while recording data at room temperature.

Lattice dynamics calculations, Orthorhombic perovskite manganite (Space group Pnma/Pbnm) shows the allowed 24 Raman active modes while Orthorhombic perovskite manganite (Space group Imma) show12 Raman active modes. Since there are no Raman-active lattice vibrations predicted in the ideal cubic Pm-3m perovskite, all phonon features in the spectra of cubic perovskite-like manganites originate from either coherent or incoherent lattice distortions.[33-35] Figure 3 shows the unpolarized Raman spectra of $CaMn_{1-x}Fe_xO_3$ (x = 0.0, 0.1, 0.2, 0.3 and 0.4) at room temperature in the spectral range 100 to 900 cm^{-1}. The Lorentzian fittings on the Raman spectra have been done to find out the exact position of the peaks (Figure 3). These peaks are tabulated in Table II &
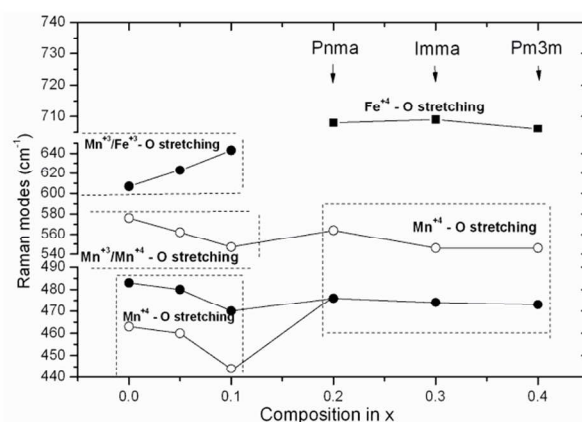
Figure 4. Combined results of synchrotron x-ray diffraction and Raman spectroscopic measurements for $CaMn_{1-x}Fe_xO_{3-\delta}$ ($0.0 < x < 0.4$).

III (supplement information). From a crystallographic point of view, stoichiometric $Ca^{2+}Mn^{4+}O_3$ has a crystal structure closest to the one of a perfect crystal. As the Mn^{4+} (t_{2g}^3) is a non-Jahn-Teller (JT) ion, the six Mn-O bonds in the MnO_6 octahedra are almost equal and the real structure (with space group Pnma) is fixed mainly by the octahedral tilts. The Raman active modes in Orthorhombic Pnma structure originate from the cubic zone boundary points Rc, Mc and Xc. While, MnO_6 octahedra deforms due to JT ion Mn^{3+} ($t_{2g}^3 e_g^1$) in $LaMnO_3$ (four shorter and two longer Mn-O bonds exists).[34-35] $CaMnO_3$ and $LaMnO_3$ compounds show the presence of mixed valences Mn^{3+} / Mn^{4+} when prepared in open air at high temperatures.[36] Raman spectra of $CaMnO_{3-\delta}$ shows the characteristic high intensity peaks due to the vibration for both Mn^{+4}-O_6 (463, 483cm^{-1}) and Mn^{+3}-O_6 (607 cm^{-1}) octahedra along with the other peaks (Figure 3&4). It shows that the JT distortion is present in the lattice due to the presence of Mn^{+3} along with the Mn^{+4}. These results have been found also by Wang et al. in $CaMn_2O_4$ where Mn remains in Mn^{+3} valence state.[37]

In $CaMn_{1-x}Fe_xO_{3-\delta}$, Raman peaks for (x=0.0-607 cm^{-1}, x=0.1 -643 cm^{-1}) have been observed due to the presence of Mn^{+3}-O and Fe^{+3}–O vibrations, while Raman peaks (for x=0.0 – 463,483 cm^{-1}, x=0.1 -444, 470 cm^{-1}) have been observed due to the presence of Mn^{+4}-O vibrations (Figure 3&4). The compositions x=0.2, x=0.3 and x=0.4 show the Raman peaks due to Mn^{+4}-O vibrations at 476 cm^{-1}, 474 cm^{-1}, 473 cm^{-1} consequently(Figure 3&4). It shows that the presence of Mn^{+3} valence state only in composition x = 0.0. The compositions x=0.2, x=0.3 and x=0.4 do not show the presence of Mn^{+3} valence state. The characteristic Mn^{+4}-O vibrations at ~460 and ~480 cm^{-1} are merged in compositions x=0.2, x=0.3 and x=0.4, this might be due to the change in space group with increase in Fe content(Figure 3&4). To find the presence of (Fe-O) vibrations in $CaMn_{1-x}Fe_xO_{3-\delta}$ ($0.1 \leq x \leq 0.4$) compositions, we have compared the Raman spectra of these compositions with the Raman spectra of $CaFeO_3$ (CFO) and $La_{0.33}Sr_{0.67}FeO_3$ (LSFO).[32, 38] The intense peak of the FeO_6 vibration found at 707 cm^{-1} and 705 cm^{-1} in the Raman spectra of CFO and LSFO, which implies that some amount of JT-type distortion is present at room temperature in CFO, indicating the existence of a JT, Fe^{+4} ionic state along with the non-JT, Fe^{+3} valence state.[38] In this study,

we have found the presence of (Fe-O) vibration modes at 715 cm^{-1} in x=0.1 composition, 708cm^{-1} in x=0.2 composition, 709 cm^{-1} in x=0.3 composition and 706 cm^{-1} in x=0.4 composition (figure 3&4). The Fe-O vibration modes show that there is a presence of

5   Fe^{+4}-O vibration mode in x=0.2, x=0.3 and x=0.4 while x=0.1 composition shows the vibrations of $Fe^{+3} - O_6$ octahedra. These observations are similar to the results have been found using synchrotron XRD patterns, where compositions x=0.2, x=0.3 and x=0.4 does not show any oxygen deficiency in lattice. Figure 4

10 summarises the results of synchrotron x-ray diffraction and Raman measurements. Further, we have followed the procedure adopted by carlos et al. to obtained mean valency of Mn and Fe in perovskites.[39] Using iodometric titration, we have found that oxygen content was 2.92 in our parent composition $CaMnO_{3-\delta}$

15 which further increased to 2.96 in x=0.1 composition. The oxygen content was found from 2.98 to 3.01 in x=0.2, 0.3 and 0.4 Fe doped compositions. It shows that the Fe is present in +4 valence state $CaMn_{1-x}Fe_xO_3$.

Figure 5 shows the magnetic moment vs. temperature (T) for

20 $CaMn_{1-x}Fe_xO_{3-\delta}$ $(0.0 \leq x \leq 0.3)$. All sample first cooled to 10K then magnetization was recorded in 1Tesla magnetic field. Magnetization of $CaMnO_{3-\delta}$ follow the Curie-Weiss law $\chi = C/(T-\theta_p)$ (where $\chi = M/H$) between room temperature to 140K. The Weiss constant θ_p is found negative(inset in fig 5), which

25 indicates the presence of antiferromagnetic interactions in the parent composition $CaMnO_{3-\delta}$. The magnetic transition temperature (Neel temperature T_N) from paramagnetic to antiferromagnetic is found 125K in our non stoichiometric bulk $CaMnO_{3-\delta}$. The magnetic transition is found broad in our non

30 stoichiometric bulk $CaMnO_{3-\delta}$ than it has been observed in stoichiometric $CaMnO_3$.[36] In stoichiometric $CaMnO_{3-\delta}$, G-type antiferromagnetic order indicates antiferromagnetic domain spin canting effects. In zero field cooled conditions at low temperatures, antiferromagnetic domains will be oriented

35 randomly. When field is increased then those domain for which antiferromagnetic polarization is perpendicular to the field dominates the magnetic response. When temperature is raised then most of the domains reoriented and the decreasing antiferromagnetic order parameter will yield smaller static spins

40 to be canted, thereby leading to a decrease in magnetization in stoichiometric $CaMnO_{3-\delta}$.

In O-deficient $CaMnO_{3-\delta}$ at low temperatures, magnetic transition is found broad and more suppressed even in 1 Tesla applied field (Figure 5).[32,36] It might be interpreted with the $Mn^{+3} - O - Mn^{+4}$

45 clusters having their net spin aligned with the overall antiferromagnetic polarization axis. Thus the spin system in the ground state is formed by the antiferromagnetic super exchange between Mn^{+4} ions and the antiferromagnetic interaction between Mn^{+3} and Mn^{+4} ions. In an external field, the preferred alignment

50 of these clusters would be along the external field direction. Thus the clusters hinder the field induced transverse reorientation of the antiferromagnetic domains. With the increase in temperature, magnetization therefore manifests the transverse response that accompanies the antiferromagnetic order parameter decreases.

55 Temperature destabilizes the G-type magnetic phase due to the weakening of the antiferromagnetic interaction between Mn^{+3} and Mn^{+4} ions, which caused by the enhancement of the double exchange and formation in the antiferromagnetic phase with
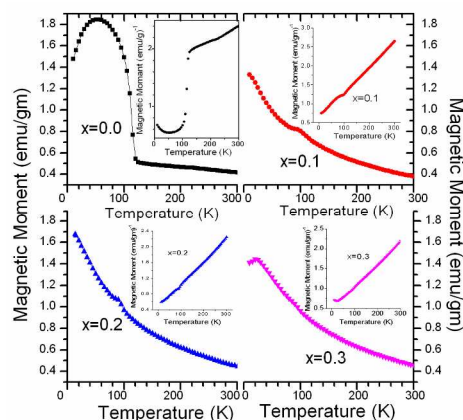
60   **Figure 5.** Magnetic properties of $CaMn_{1-x}Fe_xO_{3-\delta}$ $(0.0 \leq x \leq 0.4)$. Inset shows the inverse magnetization vs T graphs.

chains of the ferromagnetically coupled Mn^{+3} and Mn^{+4} ions. The substitution of 10% Fe at Mn site in $CaMnO_{3-\delta}$ shows the melting of antiferromagnetic state. These results are similar with the

65 reported magnetic and transport properties of $La_{0.7}Ca_{0.3}Mn_{1-x}Fe_xO_3$,[40] where it has been observed that ~10% doping of Fe at Mn site destroy the double exchange operates between Mn^{+3} and Mn^{+4} ions via O. The compositions x = 0.1 and 0.2 of $CaMn_{1-x}Fe_xO_{3-\delta}$ $(0.0 \leq x \leq 0.4)$ shows small kink at 100K and 94K in the

70 magnetization data. Below to ~ 100K, magnetization increases with the decrease in temperature. The kink in magnetization data is originated due to the competition between antiferromagnetic and paramagnetic states with the substitution of Fe at Mn site in $CaMnO_{3-\delta}$. For 30% Fe substitution at Mn site, we have not

75 observed any kink in magnetization and moment continuously increased up to 20K. We have obtained effective paramagnetic moment (P_{eff}) from the curie constant values using Curie-Weiss law. We have also calculated P_{eff}(cal) value for x=0.2 and 0.3 compositions ($4.20\mu_B$ and $4.30\mu_B$) by formula given by Taguchi

80 et al.,[41] both P_{eff} and P_{eff}(cal) values are close to the value obtained by das et al.[42] It shows that in our compositions (x=0.2, 0.3 and 0.4), Fe and Mn are present in +4 valence state. This result is similar to which has been obtained by X-ray absorption spectroscopy (XAS) and magnetic measurement by das et al and

85 Synchrotron diffraction, chemical titration, tolerance factor analysis and Raman spectroscopic studies from our results.

Impedance measurements for $CaMn_{1-x}Fe_xO_{3-\delta}$ $(0.0 \leq x \leq 0.4)$ were carried out in the frequency range 10 Hz to 10 MHz. The impedance data of all these compounds are plotted and analyzed

90 by frequency dependent ac conductivity. The frequency dependence of the conductivity for $CaMn_{1-x}Fe_xO_{3-\delta}$ (x =0.0, 0.1, 0.2, 0.3 and 0.4) compositions at room temperature is shown in Figure 6. The conductivity data of Parent $CaMnO_{3-\delta}$ show the decrease in conductivity with the increase in frequency. This

95 behavior is totally different with the observed behavior of conductivity for Fe doped samples. The Fe doped $CaMn_{1-x}Fe_xO_{3-\delta}$ (x =0.1, 0.2, 0.3 and 0.4) compositions show the increase in conductivity with the increase in frequency. At low frequencies, x=0.3 composition shows the decrease in conductivity more than

100 two orders of magnitude while other compositions x=0.1, x=0.2, x=0.4 also show the decrease in conductivity more than one order
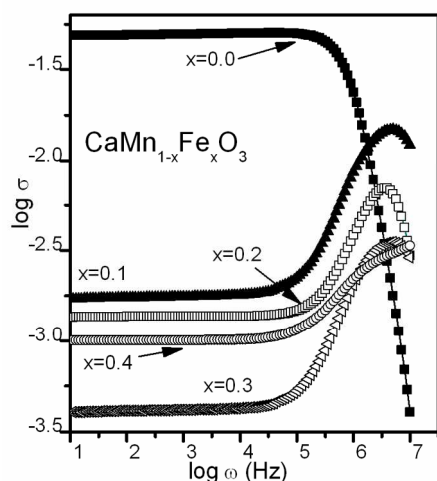
Figure 6. AC transport properties of $CaMn_{1-x}Fe_xO_{3-\delta}$ ($0.0 \leq x \leq 0.4$) samples at room temperature.

of magnitude in comparison to x=0.0 composition. The large decrease in conductivity of Fe doped compositions is found mainly due to absence of Mn^{+3} $(t_{2g}^3 e_g^1)$ in the lattice of Fe doped compositions. In $CaMnO_{3-\delta}$, it is known that the presence of double exchange interactions enhances the conductivity because of the hoping of one e_g electron of Mn^{+3} $(t_{2g}^3 e_g^1)$ in $Mn^{+3}-O-Mn^{+4}$ lattice.[32] However, according to band picture of Fe and Mn in perovskites proposed by Ahn et al., bottom of the Mn e_g band is at the same level or higher than the top of the Fe e_g band.[43] In Fe doped compositions x=0.2, 0.3 and 0.4 contains Mn^{+4} $(t_{2g}^3 e_g^0)$ and Fe^{+4} $(t_{2g}^3 e_g^1)$ valence states, Which shows that Mn e_g band is empty and e_g band of Fe is less than half filled so hopping of electron between Fe e_g band and Mn e_g band is energetically forbidden. Lack of hopping of e_g electron results the decrease in conductivity with Fe doping at Mn site in $CaMnO_3$.

Figure 7 & 8 present the frequency dependent magnetocapacitance (MC) and magnetoloss (ML) behavior at room temperature at selected magnetic fields from 1kGauss to 7.8kGauss for $CaMn_{1-x}Fe_xO_{3-\delta}$ (x = 0.0 and 0.3) compositions. Parent composition in figure 7 shows the maximum negative magnetocapacitance value -2% for low magnetic field 5kG at low frequency values. At high frequencies, MC values approaches towards zero. Figure 8 shows MC and ML behavior of x=0.3 composition. Composition x=0.3 shows the positive MC value and it has been found maximum ~8.45% for 7.8kG magnetic field at low frequency at room temperature. This type of the MC property can be explained by Maxwell Wagner (M-W) capacitor model, where two leaky capacitor in series and one of the leakage components being magnetically tuneable. In this case, oxygen deficient $Mn^{+4} - O - Mn^{+4}$ lattice is like one component and Fe doped oxygen deficient lattice is another component. It has been shown in literature that oxygen deficient lattice of $CaMnO_{3-\delta}$ can be tuned with the use of magnetic field and Fe doping blocks the double exchange mechanism which operates in manganites.[14,32,36] Lattice resistance increases with Fe doping in $Mn^{+4} - O - Mn^{+4}$ lattice and it act as a resistive layer. An important feature to note is that at low frequency the maximum of magnetocapacitance and magnetoloss curves do not exactly coincide with each other which would be expected in the case where magnetocapacitance
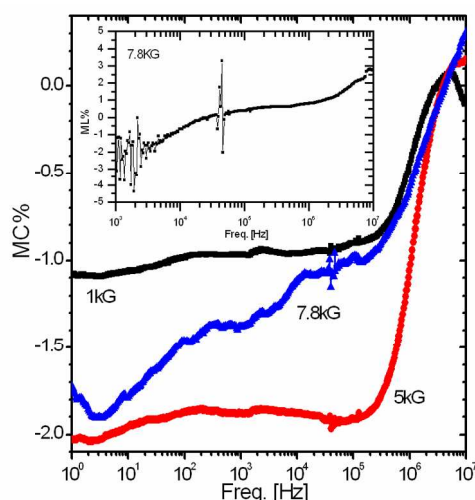
Figure 7. Magnetocapacitance (MC) and Magnetoloss (ML) properties of $CaMnO_{3-\delta}$
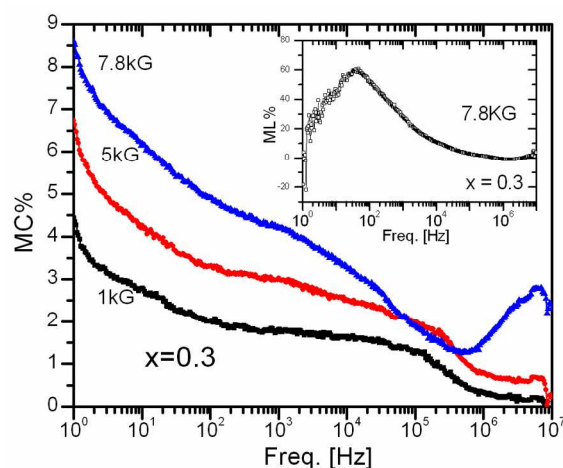
Figure 8. Magnetocapacitance (MC) and Magnetoloss (ML) properties of $CaMn_{0.7}Fe_{0.3}O_3$. Note the ~8.5% MC at room temperature at low magnetic field 7.8kG.

is completely driven by extrinsic effects. It shows that MC found ~8.45% at room temperature and at low magnetic field 7.8kG is due to the intrinsic effects. Magnetocapacitance in x=0.3 composition is originated due to the local magnetoresistance in oxygen deficient $Mn^{+4} - O - Mn^{+4}$ lattice and presence of Fe in lattice. In presence of Fe, whole sample does not show magneto resistance but local magnetoresistance might have been originated in lattice which has induced magnetocapacitance. This behavior of MC data is a basic illustration of the Maxwell-Wagner effect, where Fe in $Mn^{+4} - O - Mn^{+4}$ lattice mixes the longitudinal, transverse, real and imaging modes of the response to create an unexpected rich behavior i.e. dielectric relaxation and dielectric resonance.

Conclusions

In conclusion, we have demonstrated the Fe doping at Mn site in

perovskite $CaMnO_{3-\delta}$ brings novel effects (i) change in space group (ii) mixed valences of Fe^{+4} and Mn^{+4} for x=0.2, 0.3 and 0.4 compositions (iii) antiferromagnetic magnetic ordering turns into paramagnetic, (iii) large decrease in AC conductivity at room temperature and (iv)quit high positive magnetocapacitance at room temperature at low magnetic field and at low frequencies. Transport studies shows the insulator type of the behavior and conductivity value has been observed more than two orders of magnitude lesser in x=0.3 in compare to x=0.0. Large magnetocapacitance (MC~8.45%) at room temperature (300K) at low magnetic field (7.8kGauss) has been found in $CaMn_{0.7}Fe_{0.3}O_{3-\delta}$. Large MC value shows strong Magnetoelectric effects in x=0.3 composition is due to the presence of Fe in Mn^{+4} - O – Mn^{+4} lattice through a combination of local core magnetoresistance and Maxwell-Wagner effect.

Acknowledgments

Notes and references

Centre of Material Sciences, University of Allahabad, Allahabad - 211002
E-mail: brajendr@gmail.com; brajendr@allduniv.ac.in
Phone-+91-9451545392 Fax: +91-0532-2460017

† Electronic Supplementary Information (ESI) available: [JCPDS-XRD data and Tables of Raman spectroscopic data]. See DOI: 10.1039/b000000x/

1 S.Jin, T. H. Tiefel, M. McCormack, R. A. Fastnacht, R. Ramesh, L. H. Chen, Science, 1994, **264**, 413.

2 Colossal Magnetoresistance, Charge ordering , and related properties of manganese oxides, edited by C. N. R. Rao and B. Raveau (World Scientific, Singapore, 1998)

3 C. Zener, Phys. Rev. 1951, **82**, 403.

4 B. Singh, S. S. Manoharan, M. L. Rao and S. P. Pai Phys. Chem. Chem. Phys. 2004, **6**, 4199.

5 Q. Zhou, B. J.Kennedy, J. Solid State Chem 2006, **179**, 3568.

6 N. Hur, S.Park, P. A.Sharma, J. S.Ahn, S.Guha S.-W. Cheong, Nature (London) 2004, **429**, 392..

7 N. S.Rogado, J.Li, A. W.Sleight, M.A.Subramanian, Adv. Mater.2005, **17**, 2225.

8 P.Padhan, H. Z.Guo, P.LeClair, A. Gupta, Appl. Phys. Lett. 2008, **92**, 022909.

9 A. K.Kundu, R.Ranjith, B.Kundys, N.Nguyen, V.Caignaért, V.Pralong,; W.Prellier, B.Raveau, Appl. Phys. Lett.2008, **93**, 052906.

10 S.Mercone, A.Wahl. A.Pautrat, M.Pollet, C.Simon, Phys. Rev. B 2004, **69**, 174433.

11 J. Rivas, J. Mira, B. Rivas-Murias, A. Fondado, J. Dec, W. Kleemann M. A. Señaris-Rodríguez, Appl. Phys. Lett. 2006, **88**, 242906.

12 R.P.Rairigh, G. S.Bhalla, S.Tongay, T.Dhakal, A.Biswas, A. F.Hebard, Nature Physics 2007, **3**, 551.

13 G.Lawes, A. P.Ramirez, C. M.Varma, M. A. Subramanian, Phys. Rev. Lett. 2003, **91**, 257208.

14 R.Tackett, G.Lawes, B.C.Melot, M.Grossman, Toberer, E. S.; Seshadri, R. Phys. Rev B 2007, **76**, 024409.

15 G.Catalan, Appl. Phys. Lett.2006, **88**, 102902.

16 J. C. Maxwell, Treatise on Electricity and Magnetism (Dover, New York, 1991)

17 R. J. Wagner, Ann. Phys. (Leipzig) 1913, **40**, 817.

18 M. M.Parish; P. B.Littlewood, Phys. Rev. Lett. 2008, **101**, 166602.

19 Y. S.Shin, S. O.Park, Microw. Opt. Technol. Lett. 2010, **52**, 2364.

20 A.Reller, J. M.Thomas, D. A. Jefferson, Proc. Roy. Soc. A 1984, **394**, 223.

21 K.Vijayanandhini, T. R. N. Kutty J. Mater. Sci:Mater Electron 2009, **20**, 445.

22 C. C. K. Chiang, K. R. Poeppelmeier Mater. Lett. 1991, **12**, 102.

23 B.Singh, S. S. Manoharan Mater. Lett. 2011, **65**, 2029.

24 M. N. Iliev, M. V. Abrashev, V. N. Popov V. G. Hadjiev Phys. Rev. B 2003, **67**, 212301.

25 M.Hernando, L.Miranda, A.Varela, K.Boulahya, S.Lazar, D.C.Siclair, G.-Calbet, J. M.Parras, M. Chem. Mater. 2013, **25**, 548.

26 Q. Zhou, B. J. Kennedy Journal of Phys and Chem Solid 2006, **67,**1595

27 C. J. Howard, K. S. Knight, B. J Kennedy and E. H. Kisi J. Phys.: Condens. Matter 2000, **12**, L677

28 C. C. K.Chiang, K. R. Poeppelmeier Mater Lett. 1991, **12**, 102.

29 K.Vjayanandhini, T. R. N. Kutty J Mater Sci Mater Electron 2009, **20**, 445.

30 X.J.Liu, Z. Q. Li, P. Wu, E.Y.Jiang Solid State Commun. 2007, **142**, 525.

31 I. Guedes, J. F. Mitchell, D. Argyriou and M. Grimsditch J. Raman Spectrosc. 2000, **31**, 1013.

32 J.Briatico, B.Alascio, R.Allub, A.Butera, A.Caneiro, M. T.Causa, M. Tovar Phys. Rev. B 1996, **53**, 14020.

33 V.Dediu, C. Ferdeghini, F. C.Matacotta, P.Nozar, G.Ruani, Phys. Rev. Lett.2000, **84**, 4489.

34 M. V.Abrashev, J.Backstrom, L.Borjesson, V. N.Popov, R. A.Chakalov,N.Kolev, R.-L.Meng, M. N. Iliev Phys. Rev. B 2002, **65**, 184301.

35 J.Xu, J. H.Park, H. M. Jang, Phys. Rev. B 2007, **75**, 012409.

36 Z.Zeng, M.Greenblatt, M.Croft Phys. Rev. B 1999, **59**, 8784.

37 Z.Wang, S. K.Saxena, J. J.Neumeier, J. Solid State Chem. 2003, **170**, 382.

38 S.Ghosh, , N.Kamaraju, M.Seto, A.Fujimori, Y.Takeda, S.Ishiwata, S.Kawasaki, M.Azuma,; M.Takano; A. K. Sood Phys. Rev. B 2005, **71**, 245110.

39 C. V.-Va´zquez, M. C. Blanco, M. A. L.-Quintela, R. D. Sa´nchez, J. Rivas and S. B. Oseroff J. Mater Chem. 1998, **8**, 991

40 J. R.Sun, G. H.Rao, B. G. Shen, H. K. Wong, Appl. Phys.Lett. 1998, **73**, 2998.

41 H. Taguchi Physica B 2002, **311**, 298.

42 Neetika Das, I.A. Dhiman, A.K.Nigam, A. K.Yadav, D. Bhattacharyya, S. S. Meena, J. Appl. Phys. 2012, **112,** 123913.

43 K. H. Ahn, X. W.Wu, K. Liu, and C. L. Chein J. Appl. Phys. 1997, **81**, 5505

$Mn_{0.6}/Fe_{0.4}$
Cubic

$Mn_{0.7}/Fe_{0.3}$
Orthorhombic
show ~8% Magnetocapacitance
at 7.8kG at room temperature

Mn_1 / Fe_0
Orthorhombic
mixed valence Mn^{+3}/Mn^{+4}

Perovskite Manganite

Mn/Fe

O

Ca

$CaMn_{1-x}Fe_xO_{3-\delta}$